Characterization and preliminary imaging evaluation of a clinical prototype stationary intraoral tomosynthesis system

Christina R. Inscoe[a)]
Department of Physics and Astronomy, University of North Carolina at Chapel Hill, Chapel Hill, NC 27599, USA
Department of Applied Physical Sciences, University of North Carolina at Chapel Hill, Chapel Hill, NC 27599, USA

Enrique Platin
Department of Diagnostic Sciences, School of Dentistry, University of North Carolina at Chapel Hill, Chapel Hill, NC 27599, USA

Sally M. Mauriello
Department of Dental Ecology, School of Dentistry, University of North Carolina at Chapel Hill, Chapel Hill, NC 27599, USA

Angela Broome and Andre Mol
Department of Diagnostic Sciences, School of Dentistry, University of North Carolina at Chapel Hill, Chapel Hill, NC 27599, USA

Laurence R. Gaalaas and Michael W. Regan Anderson*
School of Dentistry, University of Minnesota, Minneapolis, MN 55455, USA

Connor Puett
Joint Department of Biomedical Engineering, University of North Carolina at Chapel Hill, Chapel Hill, NC 27599, USA

Jianping Lu and Otto Zhou
Department of Physics and Astronomy, University of North Carolina at Chapel Hill, Chapel Hill, NC 27599, USA
Department of Applied Physical Sciences, University of North Carolina at Chapel Hill, Chapel Hill, NC 27599, USA

Purpose: Technological advancements in dental radiography have improved oral care on many fronts, yet diagnostic efficacy for some of the most common oral conditions, such as caries, dental cracks and fractures, and periodontal disease, remains relatively low. Driven by the clinical need for a better diagnostic yield for these and other dental conditions, we initiated the development of a stationary intraoral tomosynthesis (s-IOT) imaging system using carbon nanotube (CNT) x-ray source array technology. Here, we report the system characterization and preliminary imaging evaluation of a clinical prototype s-IOT system approved for human use.

Methods: The clinical prototype s-IOT system is comprised of a multibeam CNT x-ray source array, high voltage generator, control electronics, collimator cone, and dynamic digital intraoral detector. During a tomosynthesis scan, each x-ray source is operated sequentially at fixed, nominal tube current of 7 mA and user-specified pulse width. Images are acquired by a digital intraoral detector and the reconstruction algorithm generates slice information in real time for operator review. In this study, the s-IOT system was characterized for tube output, dosimetry, and spatial resolution. Manufacturer specifications were validated, such as tube current, kVp, and pulse width. Tube current was measured with an oscilloscope on the analog output of the anode power supply. Pulse width, kVp, and peak skin dose were measured with a dosimeter with ion chamber and high voltage accessory. In-plane spatial resolution was evaluated via measurement of MTF and imaging of a line pair phantom. Spatial resolution in the depth direction was evaluated via artifact spread measurement. The size of the collimated radiation field was evaluated for compliance with FDA regulations. A dental phantom and human specimens of varying pathologies were imaged on a clinical 2D intraoral imaging system as well as s-IOT for comparison and to explore potential clinical applications.

Results: The measured tube current, kVp, and pulse width values were within 3% of the set values. A cumulative peak skin dose of 1.12 mGy was measured for one complete tomosynthesis scan using a 50-ms pulse per projection view. Projection images and reconstruction slices revealed MTF values ranging from 8.1 to 9.3 cycles/mm. Line pair imaging verified this result. The radiation field was found to meet the FDA requirements for intraoral imaging devices. Tomosynthesis reconstruction slice images of the dental phantom and human specimens provided depth resolution, allowing visibility of anatomical features that cannot be seen in the 2D intraoral images.

Conclusions: The clinical prototype s-IOT device was evaluated and found to meet all manufacturer specifications. Though the system capability is higher, initial investigations are targeting a low-dose range comparable to a single 2D radiograph. Preliminary studies indicated that s-IOT provides increased image quality and feature conspicuity at a dose comparable to a single 2D intraoral radiograph.

1. INTRODUCTION

Exploration into the clinical utility of dental radiography began shortly after the discovery of the x ray, with dental imaging devices evolving at a pace similar to medical radiography.[1] Intraoral radiography is currently the most commonly used imaging tool in dental clinics, often considered to be an indispensible component of dental screening and diagnosis, and the gold standard for caries detection. Improved efficiency of intraoral receptors, including film, photostimulable phosphor plates, and direct flat panel detectors, has greatly reduced the amount of radiation required to obtain images of diagnostic quality. Unfortunately, the features of interest within the dental anatomy are often obscured by superposition of bone, teeth, restorations, and dental hardware. This superposition is a fundamental limitation due to the 2D nature of projection radiography and results in low diagnostic accuracy for many tasks.[2] Sensitivity of caries detection ranges from 40 to 70%, depending on the accessibility of the lesion.[3,4] Root fracture detection is another application of 2D intraoral radiography that is lacking sensitivity, with features often obscured by adjacent anatomy.[1,5,6]

Computed tomography (CT) is a three-dimensional (3D) modality that reduces the problem of anatomical superposition by acquiring 2D projection images from many different angles and utilizing a reconstruction algorithm to compute a 3D representation of anatomy, presented as a collection of slice images. Cone-beam CT (CBCT) has been incorporated into many dental clinics for treatment planning, including endodontic treatment, implant site assessment, and evaluation of temporomandibular joint disorders.[1] Though valuable for diagnostic applications, CBCT is not appropriate as a screening tool. The increased radiation dose to the patient, clinician time, and equipment cost outweigh the marginal increase in sensitivity for caries detection.[7]

Limited angle tomography, or tomosynthesis, is a quasi-3D modality using reduced angular coverage, fewer projection images, and lower dose than CT. In the late 1990s, Webber et al. explored a limited angle intraoral tomography technique referred to as Tuned Aperture Computed Tomography (TACT).[8–10] TACT utilizes an intraoral detector and a standard 2D x-ray source to acquire projection images of a single region of interest at various angularities. Use of a fiducial marker[8,11] on the buccal surface of the tooth allows calculation of source/detector geometry. A reconstruction algorithm generates slice images containing some depth information. TACT demonstrated improved sensitivity in the detection of root fractures and periodontal bone loss over conventional 2D intraoral imaging and was found to be useful during evaluation of implant sites and third molar impaction.[12–20] Investigations of TACT for caries detection produced varying results.[17–21] Although

TACT clearly demonstrated the clinical benefits of tomosynthetic dental imaging and resulted in several patented technologies, it was never translated for clinical use, due to its technical limitations including the long imaging time and the use of the fiducial marker. Tomosynthesis has also been explored by use of a rotating-gantry, or C-arm, for x-ray source translation to precisely define the geometrical relationship with a fixed intraoral[22] or extraoral detector.[23,24] Systems have also been proposed that utilize mounting fixtures for source translation around a predefined path with a fixed focal point.[25] Hindered by source and receptor capabilities and computational power of the era, TACT and tomosynthesis were great ideas ahead of their time. Twenty years of evolution in source, receptor, and computer technology revives an imperative to investigate dental applications of tomosynthesis.

Until recently, accomplishing tomosynthesis required physical motion of a conventional x-ray tube, often through a line or an arc, to acquire projection images from different viewing angles. Conventional x-ray tubes emit electrons from a single thermionic cathode, generating x-ray radiation from a small focal spot on the anode. In an alternative phenomenon known as field emission, CNT cathodes generate electrons without heat, when moderate voltage is applied. The production of electrons without heat loading allows for the construction of spatially distributed, multibeam field emission x-ray source arrays.[26] Using source array architecture, an object can be imaged from multiple angulations quickly and without any mechanical motion, offering better spatial resolution and shorter scan time compared to conventional tomosynthesis. Task-specific CNT-enabled stationary tomosynthesis devices have been developed for breast[27] and chest[28] imaging and are now enrolling patients in human studies.

Recognizing the potential implications of source array technology in dental imaging, stationary intraoral tomosynthesis (s-IOT) was proposed[29] and assessed using a benchtop CNT-source array (XinRay Systems, Morrisville, NC), dental phantoms and extracted teeth, and a standard intraoral detector (SuniRay2, Suni Medical Imaging, Inc., San Jose, CA, USA).[30] Various angular spans and dose distributions were explored to define the optimal imaging configuration. Using this benchtop device, a preliminary reader study compared the detection sensitivity of s-IOT and standard 2D intraoral radiography for interproximal caries in extracted human teeth, using micro-CT images as the ground truth. Eight experienced dentist readers were 36% more likely to identify a carious lesion when viewing images generated by s-IOT compared to standard 2D intraoral radiography.[31] Encouraged by this statistically significant finding, XinVivo, Inc. (Morrisville, NC) has designed and constructed a clinical

prototype for use in the dental clinic. The University of North Carolina (UNC) Institutional Review Board (IRB) has approved the use of the device for a patient trial evaluating caries detection.[32] The purpose of this work is to perform system characterization of this s-IOT device and explore the potential range of its clinical application prior to human studies.

2. MATERIALS AND METHODS

2.A. The s-IOT system

2.A.1. System configuration

The first generation s-IOT clinical prototype system (Xin-Vivo, Inc.) was designed to mimic a typical 2D intraoral x-ray device currently used in dental clinics [Fig. 1(a)]. The CNT x-ray source array with an x-ray collimator is mounted on an articulating arm attached to the wall. A customized bitewing holder magnetically couples a standard digital intraoral detector to the exit window of the collimator and maintains a fixed source-to-image distance (SID) of 400 mm, which creates an optimum geometry for the source array and satisfies the required separation between the x-ray source and patient. The operator specifies the imaging parameters using a graphical interface [Fig. 1(b)] and a customized electronic switching system adjusts the x-ray output and synchronizes each exposure with the integration window of the digital detector.

2.A.2. The x-ray source array

The s-IOT x-ray tube is similar to a conventional dental tube in terms its physical appearance, dimensions, tube voltage, and current. However, unlike the standard single source tube, the s-IOT tube contains seven individually addressable, spatially distributed x-ray emitting focal spots, providing an angular span of approximately 12 degrees at the optimized SID of 400 mm. The x-ray tube operates at an anode voltage of 70 kV, with each x-ray source configured to produce 7 mA of tube current. The exit window provides 2 mm of aluminum filtration. These parameters are similar to those used in conventional 2D intraoral radiography. The beam on-time for each source is variable, producing a range of exposure levels. The source array is equipped with a collimator cone to limit each x-ray exposure to the detector active area only. Figure 2 is a computer-aided design model of the s-IOT source array with the collimator cone and bitewing detector holder.

2.A.3. X-ray detection

The s-IOT system utilizes an adult (size-2) digital intraoral CMOS x-ray sensor with an active area of 35.52×26.64 mm (1920 $\times$ 1440 pixels, each measuring 18.5×18.5 um). The sensor was customized specifically for s-IOT acquisition. The sensor is mounted in a custom holder, which magnetically couples to the end of the collimator cone to maintain the desired source-detector geometric relationship, with a frame rate of 1.3 cycles/s.

2.A.4. Geometric calibration

Maintaining a precise alignment and optimized distance between the x-ray sources and detector is critical for tomosynthesis reconstruction. The s-IOT system currently utilizes the manufacturing specifications of the source array geometry, collimator, and detector holder to define the source-detector geometry.
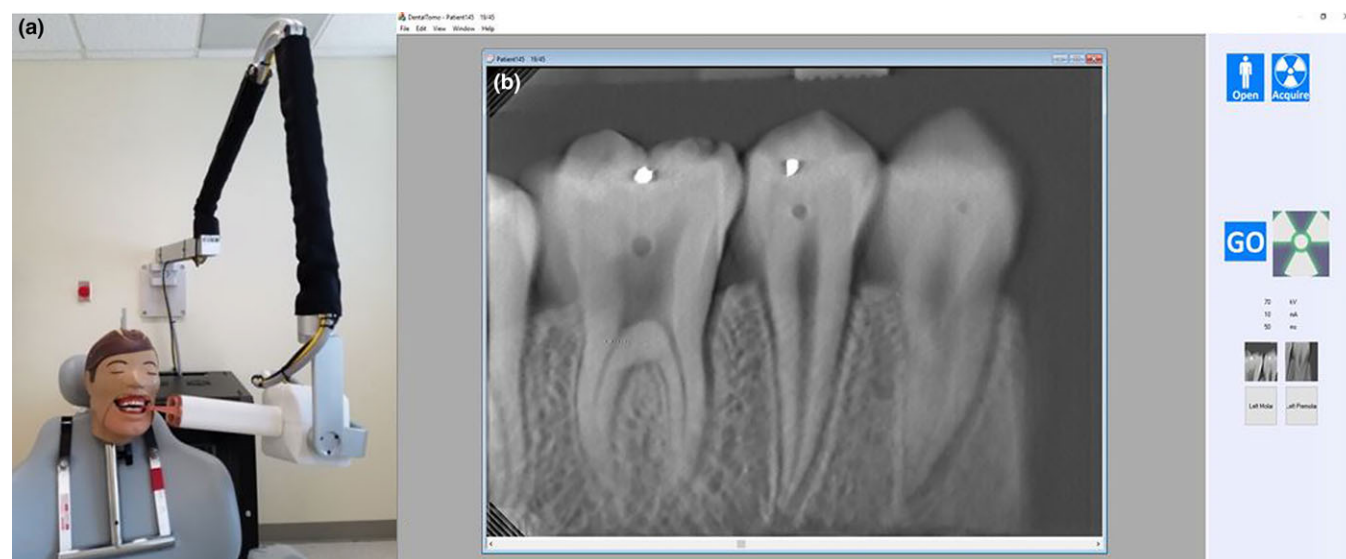

Fig. 1. (a) The first generation s-IOT clinical prototype (XinVivo, Inc.) installed in the UNC Dental Clinic. (b) The s-IOT graphical user interface (GUI) for image acquisition. [Color figure can be viewed at wileyonlinelibrary.com]
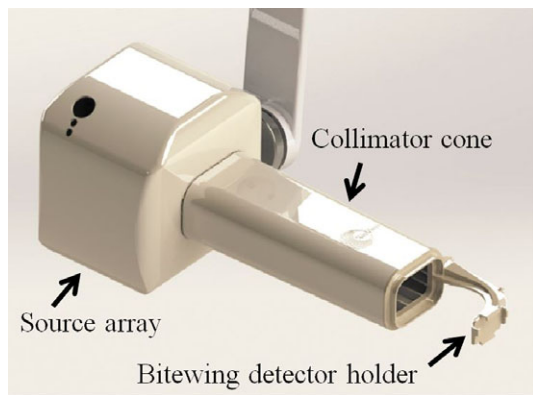
FIG. 2. s-IOT system computer-aided design model illustrating the source-detector geometry and collimator configuration. [Color figure can be viewed at wileyonlinelibrary.com]

2.B. Image processing

2.B.1. Projection image correction

The s-IOT image processing software accepts projection images sequentially from the detector and utilizes a library of previously acquired images to perform gain and offset corrections. The corrected projections are saved and displayed in real time, so that the operator can confirm that the specific area of interest is in the field-of-view. These corrected projections are used to reconstruct the 3D image space.

2.B.2. Reconstruction

Reconstruction refers to the processing steps by which the 2D information available from the projection views is used to mathematically construct a 3D image space displayed for viewing. The s-IOT system uses a proprietary simultaneous algebraic reconstruction technique developed by XinVivo with a computational time of approximately 10 s when performed on a standard PC equipped with a low-end GPU.[33] In this s-IOT system, reconstruction is performed immediately following the scan and displayed for the clinician. The result is presented as a stack of reconstructed image slices through which the reader scrolls. Each reconstruction stack contains 45 image slices, with each slice representing 0.5 mm of object thickness.

2.C. Tube current verification

System output of the source array was verified by measurement of the tube current. The amplitude and pulse width was measured for each source in the array with an oscilloscope (Tektronix TDS2001C) using the analog output of the anode power supply.

2.D. Dosimetry

Dosimetric characterization was carried out using a dosimeter (Accu-Pro, Radcal Corporation, Monrovia, CA,

USA). An accessory sensor (Accu-kV, Radcal Corporation) and aluminum standards were used to measure the half-value layer (HVL) to verify the presence of adequate beam filtration. Actual pulse widths and peak skin doses were measured using a general purpose ion chamber (Model 10x6-6, Radcal Corporation, Monrovia, CA) with digitizer (Model 9660, Radcal Corporation, Monrovia, CA). The system was evaluated at a constant tube current of 7 mA, with exposure times ranging from 25-50 ms per source. The peak skin dose was measured for each beam when pulsed at 50 ms.

2.E. Collimation

In order to limit unnecessary patient dose, the Food and Drug Administration (FDA) requires x-ray devices be properly collimated, depending on the application. Regulation 21CFR1020.31(f)(1)(i)[34] states that the radiation field of intraoral x-ray devices should be contained within a 7-cm diameter circle when imaged at the minimum source-to-skin distance. To evaluate the field size, a large photostimulable phosphor (PSP) plate receptor (ScanX Intraoral PSP, Air Techniques, Melville, NY) was placed at the output window of the collimator cone and exposed. The plate was scanned with a resolution of 30 × 30 μm pixel size on a digital radiography system (ScanX, Air Techniques, Melville, NY) and converted to a DICOM image for analysis.

2.F. Assessing image quality and potential clinical utility

2.F.1. In-plane spatial resolution

The in-plane spatial resolution was evaluated by determination of the modulation transfer function (MTF) and imaging a line pair phantom. The MTF was determined using a 100 μm-thick tungsten edge positioned at 1 cm from the active detector layer at a slight angulation[35] and imaged in two orientations, both parallel and orthogonal to the spatial distribution of x-ray sources [Fig. 3(a)]. Image gray levels were sampled to define the edge spread function (ESF), from which the MTF curve was calculated and the 10% MTF determined. The line pair phantom (Cardinal Health, Model 07-539) was also imaged in both parallel [Fig. 3(b)] and orthogonal orientations to the source array at 1 cm from the detector surface. The MTF and line pair evaluations were performed on central projection images and plane-of-focus reconstruction slices.

2.F.2. Artifact spread function

The depth resolution was evaluated by determination of the artifact spread function (ASF). An acrylic phantom containing two layers of 1 mm stainless steel spheres (Fig. 4) was imaged at 40 ms pulse width. The reconstruction was performed at the standard slice thickness representation of 0.5 mm. Object and background ROI were established that encompassed the full region of the artifact spread. The ASF
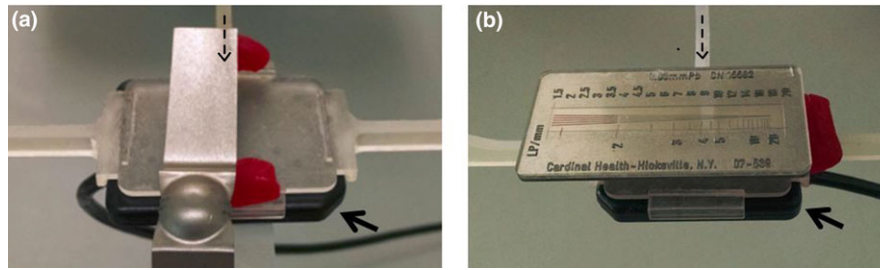
FIG. 3. (a) A tungsten edge was imaged for MTF calculations in the parallel (shown) and orthogonal directions. (b) A line pair phantom was imaged to validate image spatial resolution in both parallel and orthogonal (shown) directions. The detector, indicated with a solid arrow, is mounted in the specimen holder. The direction of incident radiation is indicated with a dashed arrow. [Color figure can be viewed at wileyonlinelibrary.com]

was computed according to Eq. (1), in which the mean pixel value (MPV) was measured in the artifact ($MPV_{artifact}$) and background (MPV_{BG}) regions for each slice (z) and feature ($MPV_{feature}$) region measured in plane-of-focus of the sphere (z_0).[36]

$$ASF(z) = \frac{MPV_{artifact}(z) - MPV_{BG}(z)}{MPV_{feature}(z_0) - MPV_{BG}(z_0)} \qquad (1)$$

2.F.3. Imaging dental phantoms and tooth specimens

The potential clinical utility of the s-IOT system was explored over a range of dental pathologies (Fig. 5) by imaging a dental quality assurance phantom (RMI 501A, Radiation Measurements, Inc., Middleton, WI, USA), extracted human teeth, and a Dental X-ray Teaching and Training Replica (DXTTR, Dentsply Rinn Corporation, York, PA, USA). The RMI phantom contains three segments of metal mesh, four thicknesses of bone mimic, and a human maxillary specimen with teeth containing metallic fillings and simulated caries lesions. The DXTTR phantoms contain cadaveric dentition with various lesions and are equipped with a mechanical bite apparatus. Figure 5(b) is a photo showing the occlusal surface of a fracture-containing tooth specimen embedded in plaster alveolar bone analog prepared by our collaborators at the University of Minnesota (UMN)
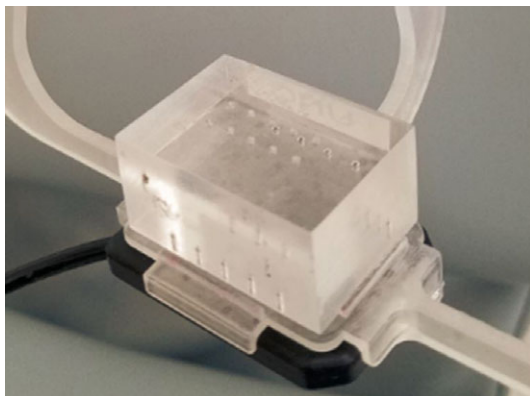

FIG. 4. Acrylic phantom with 1 mm stainless steel spheres for artifact spread measurement. [Color figure can be viewed at wileyonlinelibrary.com]

School of Dentistry. Figure 5(c) shows the dilacerated root specimens, one with an extremely curved root (arrow). Figure 5(d) is the DXTTR training phantom positioned for bitewing image acquisition.

For imaging phantoms and loose specimens, the x-ray assembly was oriented vertically and the phantom or specimen was placed on the upper surface of a detector holder designed specifically for this purpose [Fig. 6(a)]. Root fracture specimens were embedded in a plaster/walnut mix to account for attenuation due to bone and simulate marrow spaces. A 1 cm slab of dental wax represented soft tissue attenuation, Fig. 6(b). The tomosynthesis projection images were acquired at 70 kV with each source driven at 7 mA for 50 ms per projection resulting in an x-ray on-time of 350 ms for one complete tomosynthesis study. This exposure is within the range of exposure used for a single bitewing image acquisition at the UNC School of Dentistry Oral and Maxillofacial Radiology Clinic. Root fracture specimens were imaged in multiple orientations to assess fracture conspicuity at various viewing angles. Two different sample orientations are displayed in Fig. 6. For comparison, standard 2D images were acquired using a clinical 2D intraoral x-ray source (Instrumentarium Focus, Intrumentarium Dental, Charlotte, NC). The s-IOT sensor is fully integrated into the system and could not be operated independently, so photostimulable phosphor (PSP) plate receptors (ScanX Intraoral PSP, Air Techniques, Melville, NY) were used for 2D root fracture imaging. Exposures were optimized by an expert dental radiologist over a range from 320 to 500 ms at the same kV and mA. Exposed PSPs were scanned with a resolution of 30×30 μm pixel size on a digital radiography system (ScanX, Air Techniques, Melville, NY).

3. RESULTS

3.A. Tube current consistency among sources

The tube current and pulse width for each x-ray source was measured with an oscilloscope and found to be uniform with nearly square profiles. The current ranged from 6.8 to 7.6 mA, with mean amplitude of 7.2 mA, slightly exceeding the manufacturer-set value of 7 mA by <3%. The pulse widths (exposure times) of each source were uniform. Figure 7 is a profile plot displaying tube current of each x-
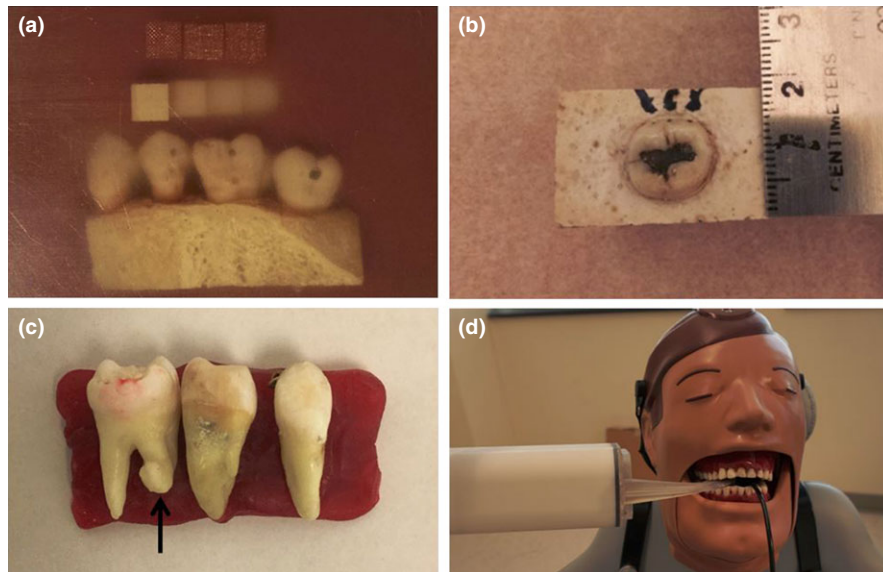
FIG. 5. Photos of the RMI phantom (a), a specimen containing fractures (b), and dilacerated roots (c). DXTTR, containing caries and other dental lesions, shown with the s-IOT source positioned for right molar bitewing imaging (d). [Color figure can be viewed at wileyonlinelibrary.com]
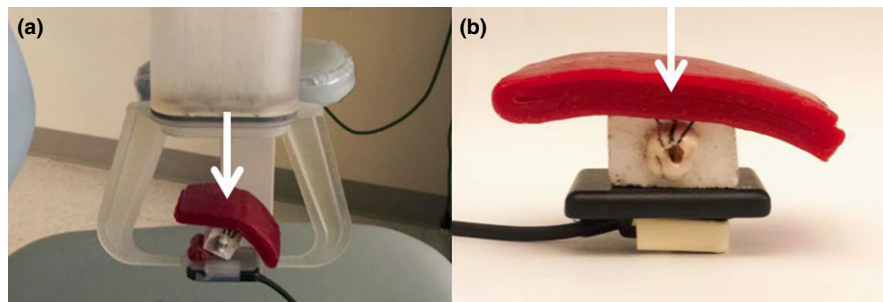

FIG. 6. (a) System configuration for phantom and specimen imaging; (b) specimen covered with a soft tissue mimic and placed on detector. The direction of incident radiation is indicated by the arrows. [Color figure can be viewed at wileyonlinelibrary.com]

ray source when pulsed at 50 ms during a complete tomosynthesis scan.

3.B. Dosimetry

The tube voltage and half-value layer (HVL) of the source array was measured using the dosimeter with kilo-voltage

FIG. 7. Pulse profiles of tube current for one tomosynthesis scan (50 ms per exposure). Each pulse represents an individual x-ray source within the array. Profiles are similar, with small variations in amplitude. [Color figure can be viewed at wileyonlinelibrary.com]

accessory and found to be 69.4 kVp and 2.9 mm of aluminum, respectively. The ion chamber was used to measure the actual pulse width of the first x-ray pulse at each output setting, confirming accurate beam on-time. (Table I). The peak skin dose was also measured for each of the seven x-ray beams when pulsed at 50 ms (Fig. 8). The average peak skin dose was 160 µGy per pulse with a cumulative dose of 1.12 mGy.
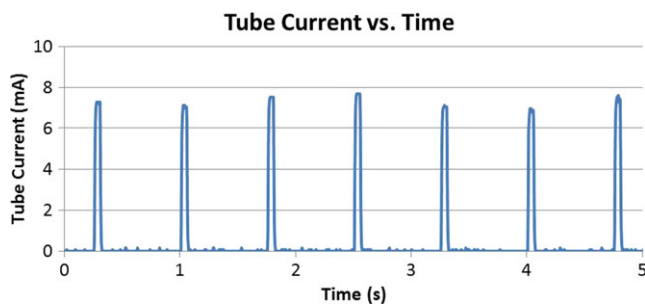
3.C. System spatial resolution

3.C.1. Modulation transfer function

The modulation transfer function (MTF) of the system was calculated for both the scanning (parallel to the x-ray source array) and orthogonal directions in both projection images as well as reconstruction slices. The projection images from the central x-ray beam demonstrate a 10% MTF at 9.1 and 9.3 cycles/mm, in the scanning and orthogonal directions, respectively. Similar results were obtained from the peripheral x-ray sources. The 10% MTF in the

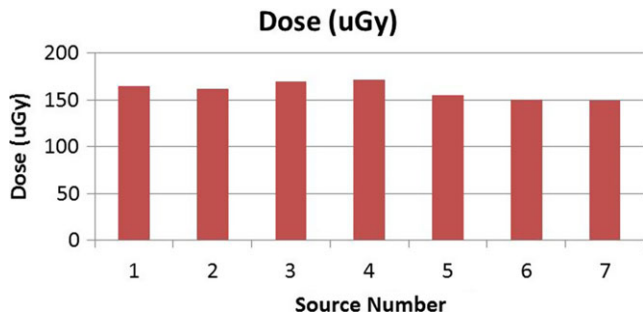| Pulse width		
Pulse width setting (ms)	Measured pulse width (ms)	Deviation (%)
25	25.2	0.8
30	29.8	0.7
35	36.2	3.4
40	40.2	0.5
45	44.9	0.2
50	50.1	0.2

FIG. 8. Plot of peak skin dose vs source number for each x-ray source in the s-IOT system. [Color figure can be viewed at wileyonlinelibrary.com]
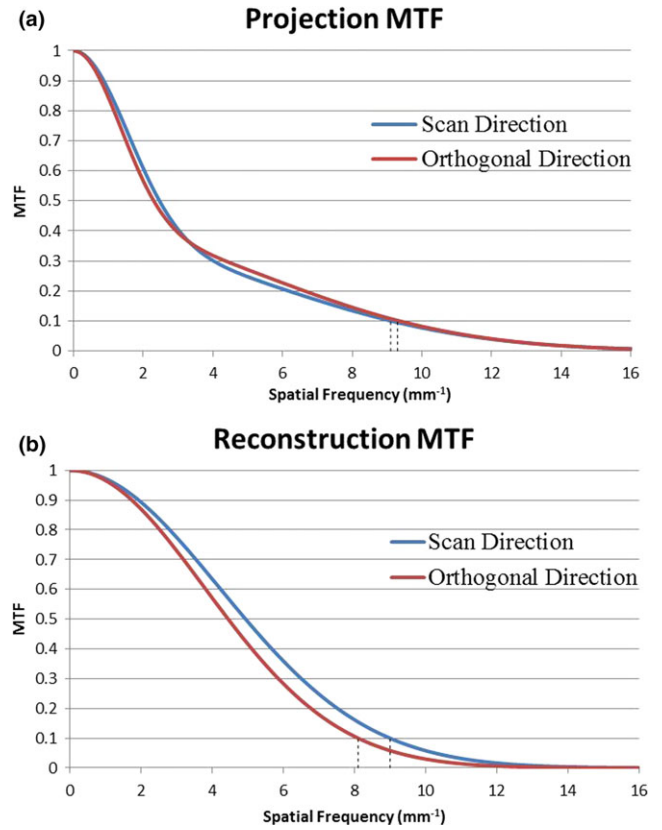

FIG. 9. Projection (a) and reconstruction (b) MTF in both scan and orthogonal directions. Dashed lines indicate the 10% cutoff values. Projection MTF was evaluated using the central x-ray beam of the source array. Reconstruction MTF was evaluated in the slice containing the focused tungsten edge. [Color figure can be viewed at wileyonlinelibrary.com]

reconstruction slice containing the in-focus tungsten edge was calculated to be 9.0 and 8.1 cycles/mm in the scanning and orthogonal directions, respectively. MTF plots are shown in Fig. 9 with dashed lines indicating the 10% cutoff value.

3.C.2. Line pair imaging

From the line pair phantom measurement, the system was found to have visual distinction >11 line pairs per mm (lp/mm) in the scanning direction, and >12 lp/mm in the orthogonal direction in the projection images. Line pair spatial resolution was consistent among all projection images of each cohort. The reconstruction slices in which the phantom was in-focus were also assessed and found to have >8 lp/mm in both the scanning and orthogonal directions. Figure 10 shows line pair projection images (inverted; 10a, 10b) and reconstruction slice images (10c, 10d). Figures 10(a) (projection image) and 10 d (reconstruction slice) indicate regions of interest at 11 and 8.5 line pairs, respectively. This line pair spacing is approaching the upper limit of visual distinction. A plot profile of each region is shown in Figs. 10(e) and 10(f), revealing five distinct peaks.

3.C.3. Artifact spread

The ASF was calculated from Eq. (1) for each slice of the reconstruction. The MPV was calculated using only the pixels exceeding the background gray level in order to remove

the impact of undershoot artifacts in the scanning direction. The plane-of-focus slice is shown in Fig. 11(a) and the outermost slice is shown in Fig. 11(b). The computed ASF values and fourth-order Gaussian fit are shown in the plot in Fig. 11(c). The FWHM is 8 mm.

3.D. Collimation

The radiation field of the s-IOT source array was evaluated for compliance with the FDA regulation for intraoral devices and found to be acceptable. Figure 12 shows the image of the scanned PSP with the 7 cm diameter ROI to indicate the maximum field dimensions. The x-ray field is 4.8 × 2.1 cm, with a maximum of 5.2 cm on the diagonal.

3.E. Dental phantom and human specimen imaging

3.E.1. RMI phantom

Images of the RMI phantom are shown in Fig. 13. A 2D radiograph is shown in Fig. 13(a). Though not apparent in the 2D image, the central and right teeth in the RMI phantom each contains three roots, two buccal roots, and one palatal root. Figure 13(b) is a drawing of such a molar to clarify this geometry. When viewed distally, the dashed lines represent
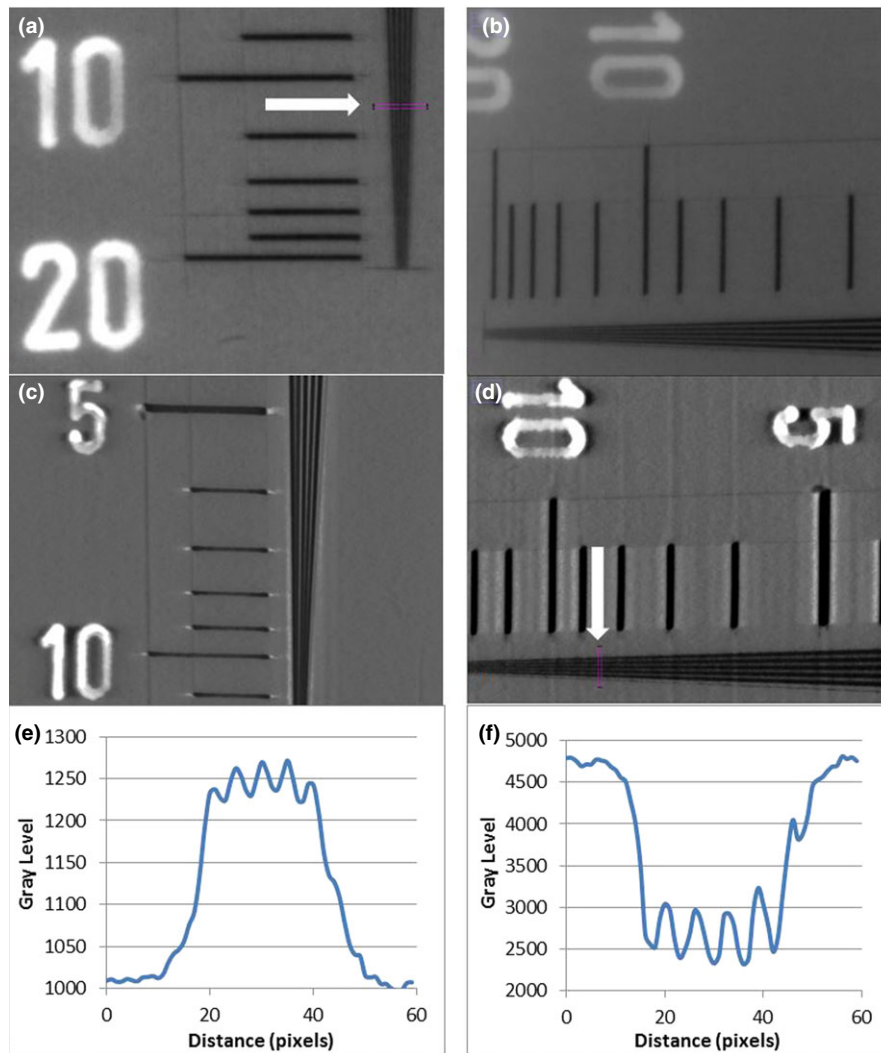
FIG. 10. Cropped projection images of the line pair phantom, oriented orthogonal to the scanning direction (a) and parallel to the scan direction (b). The arrow (a) indicates the ROI at 11 lp/mm, corresponding to the plot in Fig. 10(e). Corresponding cropped reconstruction slice images of the line pair phantom (c and d). The arrow (d) indicates the ROI at 8.5 lp/mm, corresponding to the plot in Fig. 10(f). [Color figure can be viewed at wileyonlinelibrary.com]

the tomosynthesis reconstruction slice locations in Figs. 13(c) and 13(d). Figure 13(c) is the slice in the plane of the caries lesions and allows visualization of the buccal roots of the first molar. Figure 13(d) is 15 slices (7.5 mm) posterior and is in the plane of focus of the palatal root of the first molar tooth. A Y-shaped crown fracture (white arrow) is revealed in the central tooth that is not visible in the 2D image or upper reconstruction slice.

3.E.2. Fractured root specimens

Specimens with root fractures prepared at the UMN School of Dentistry were imaged at the UNC School of Dentistry with both 2D intraoral radiography and s-IOT. Though tomosynthesis scans were performed with several sample orientations, the following images are from the standard scanning configuration, with the sample placed flush on the detector with the scanning direction orthogonal to its long axis [Fig. 6(b)]. Two example specimens are shown in

Fig. 14. Figures 14(a) and 14(b) are 2D images of the two root specimens, with the corresponding reconstruction slices shown in Figs. 14(c) and 14(d). Though the 2D images were taken with a much longer exposure, 500 ms, the root fractures are subtle and could be mistaken for adjacent root canals. The reconstruction slices exhibit higher contrast and excellent delineation of the fractures. Scrolling through the reconstruction stack allows the viewer to visualize the propagation of the fracture through the root.

3.E.3. Dilacerated root specimen

Nearly all teeth have some amount of curvature, and such dilacerations can range from slight to severe. Dilacerated roots are not an unusual finding in patient images. Assessing the direction and degree of dilacerations is critical in the delivery of endodontic treatment, orthodontic movement, or surgical intervention. Tomosynthesis is promising in these regards. Figure 15 contains sample images of one dilacerated
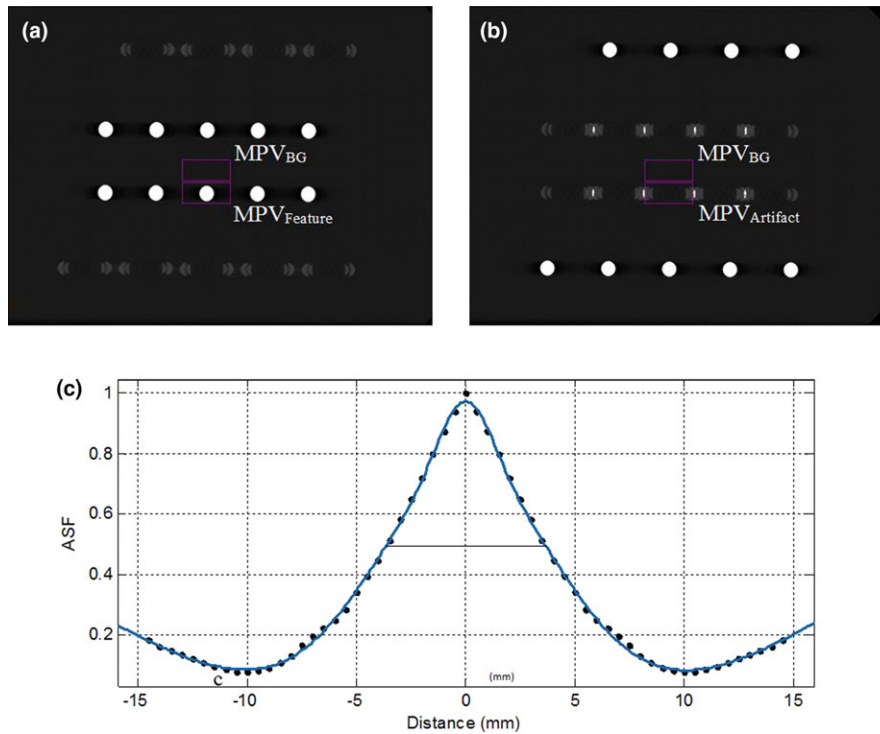
FIG. 11. (a) Reconstruction slice in the plane-of-focus of the stainless steel sphere. (b) Reconstruction slice out of the plane-of-focus of the stainless steel sphere. (c) Plot of ASF vs distance (mm) with a fourth-order Gaussian fit. [Color figure can be viewed at wileyonlinelibrary.com]
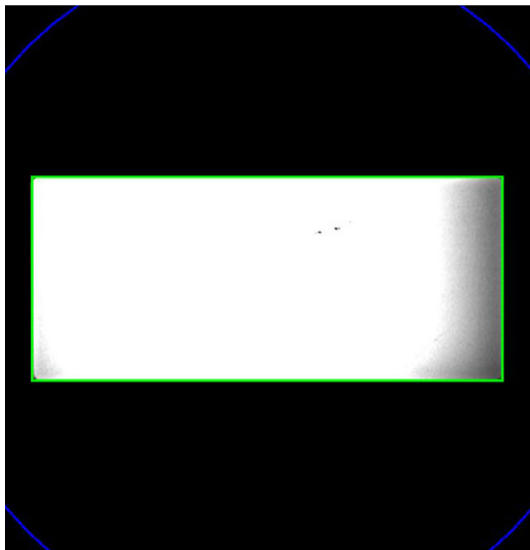

FIG. 12. Image of radiation field of s-IOT device taken with a size 4 PSP. The rectangular ROI indicates the actual field size. The circular ROI indicates the maximum size allowable by the FDA. [Color figure can be viewed at wileyonlinelibrary.com]

root specimen, the left most tooth in Fig. 5(c). The 2D radiograph is shown in Fig. 15(a). The tooth contains obvious root dilacerations, but the direction and degree of curvature are unknown due to the lack of depth information. Figures 15(b) and 15(c) are the corresponding reconstruction slices. Figure 15(b) is a slice in the plane-of-focus of the root canals and pulp and Fig. 15(c) is six slices (3 mm) anterior in the

plane-of-focus of a well-defined root tip protruding toward to the source, or in a buccal direction.

3.E.4. DXTTR image quality

The acquisition of DXTTR images required use of the bitewing detector holder, shown in Fig. 5(d). A comparison between sample 2D bitewing images and corresponding reconstruction slice images is shown in Fig. 16. The 2D bitewing images were acquired with a clinical adult size digital CMOS sensor (Schick 33, Sirona Dental Inc., Long Island City, NY). The Schick sensor contains 15 µm pixels in a 2400×1708 array, therefore has slightly higher intrinsic spatial resolution and larger FOV than the s-IOT receptor. Figures 16(a) and 16(b) are the 2D images of the molar and premolar regions, respectively. The corresponding reconstruction slices are shown in Fig. 16(c) and 16(d). The 2D image of the molar region (a) reveals a vertical crown fracture in a maxillary molar, indicated with an arrow. The corresponding reconstruction slice (c) displays the same fracture, but with higher contrast, and displays an additional fracture in the second right mandibular molar. The 2D image of the premolar region (b) reveals two fractures in one mandibular molar and one premolar. This image also displays five closed contacts (circled), in which the interproximal surfaces are superimposed and cannot be viewed individually. The corresponding reconstruction slice image (d) reveals an additional fracture in the first molar. The elimination of superposition in the slice image also opens the contacts for independent visualization of each interproximal surface.
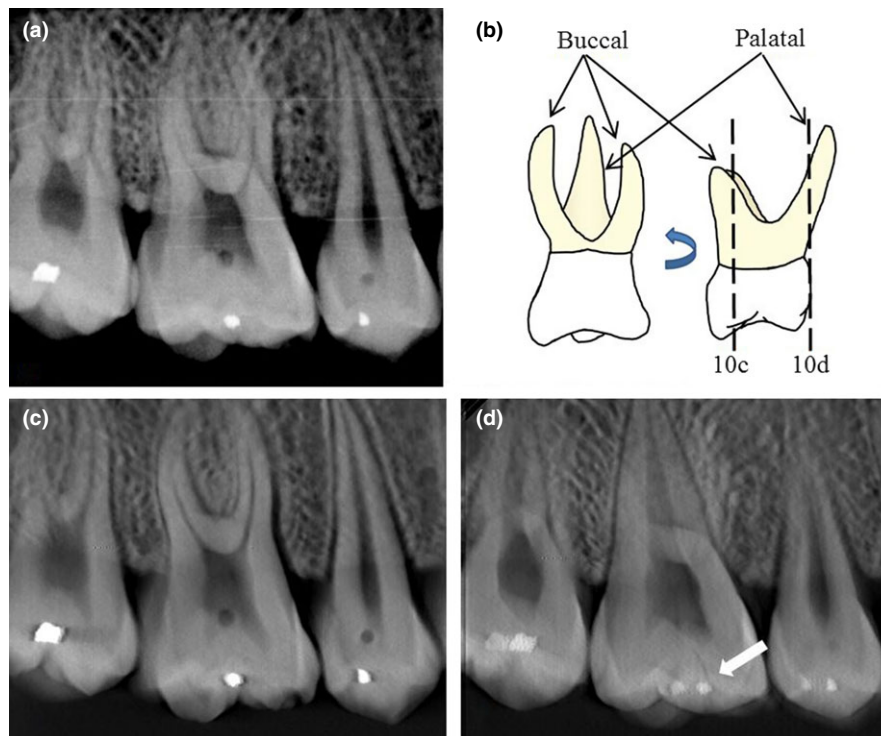
Fɪɢ. 13. (a) 2D image of the RMI phantom; (b) Drawing of a molar containing three roots; dashed lines indicate planes of focus for reconstruction slices in (c) and (d); (c) Reconstruction slice in the plane of the buccal roots, simulated caries lesions, and metallic restorations; (d) Reconstruction slice in the plane of the palatal root and a crown fracture (arrow). [Color figure can be viewed at wileyonlinelibrary.com]

4. DISCUSSION

The purpose of this study was to characterize the s-IOT clinical prototype system and to demonstrate the clinical relevance.

4.A. Tube current

The tube current was measured with high temporal accuracy on an oscilloscope and found to have a very uniform pulse width. The amplitude displayed some source-to-source variation and the average was slightly higher than the target of 7 mA, at 7.2 mA (<3%). This result is repeatable and therefore does not imply any instability in the tube, but rather is a result of the precision of the current version of the prototype electronics.

4.B. Dosimetry

The anode voltage was verified to be within 1% of the specified value of 70 kVp. The HVL of the beam was measured to be 2.9 mm Al, satisfying the regulatory requirement of HVL >1.5 mm Al for 2D intraoral sources.[37] The pulse width (exposure time) was accurate for all six settings. The largest deviation noted was 3%, with all other measurements falling within 1% of the desired width.

The peak skin dose was measured at the highest pulse width setting allowed by the acquisition software, 50 ms per source. Some source-to-source dose variation was observed that mimics the variation displayed in the tube current. At the highest exposure setting, the peak skin dose produced by the system is 1.1 mGy, and falls within the range of a single clinical 2D PSP exposure (1.0–3.3 mGy) used in the UNC School of Dentistry. The maximum exposure setting of 50 ms per pulse is designed to examine the utility of low-dose intraoral tomosynthesis for screening. The present dental CNT x-ray source array has the capability of achieving pulse widths greater than 200 ms per pulse.

4.C. Spatial resolution

The s-IOT system spatial resolution was characterized by calculation of the MTF as well as imaging of a line pair phantom, and artifact spread. The MTF values for projection images and line pair phantom projection images displayed minimal variation with respect to scan direction. The MTF values for reconstruction slices and line pair reconstruction slice images displayed a small direction-dependent variation. This variation is due to edge enhancement resulting from tomosynthesis artifacts in the scan direction. The artifact is easily visualized as bright streaking in reconstruction images of the line pair phantom, Figs. 10(c) and 10(d), and is more pronounced compared to the anatomical images due to the high contrast of the features. Spatial resolution of reconstruction slice images is >8 lp/mm for both MTF and line pair images.

The artifact spread was evaluated with a phantom containing 1 mm stainless steel spheres. This is highly attenuating
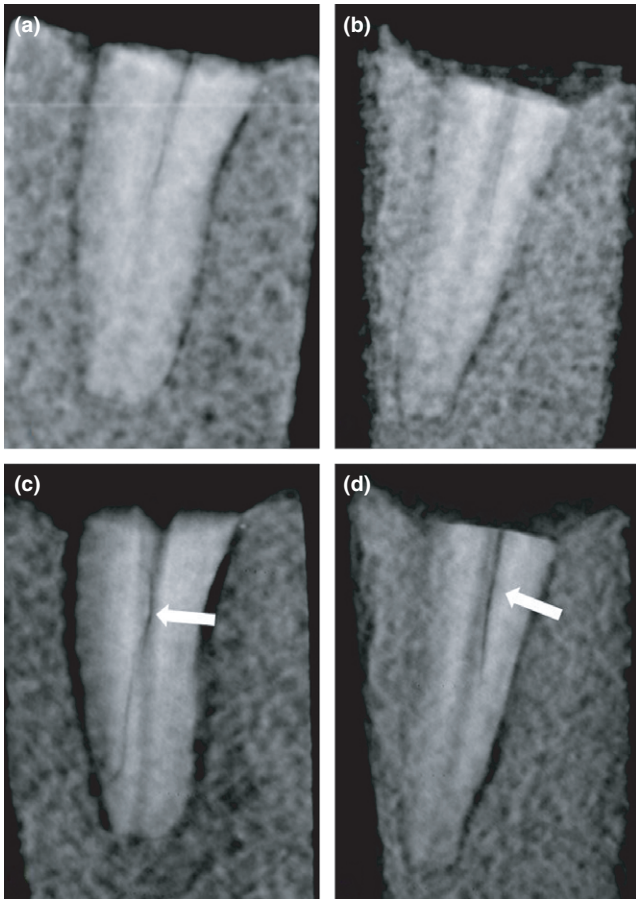
FIG. 14. (a,b) 2D images of root fracture specimens; (c,d) Corresponding reconstruction slice images reveal well-defined fractures indicated by arrows.

and relatively large in comparison to the image size, producing substantial artifact. The result shown here indicates that the impact of such artifact can reach 5 mm on either side of the object. Similar results are expected for teeth containing metallic restorations and work is underway to incorporate artifact reduction into the clinical reconstruction algorithm.

The system spatial resolution in the reconstruction slices is affected not only by the inherent properties of the detector and x-ray source, but also the geometric calibration of the

system. Precise location of the seven focal spots with respect to the detector center is required by the reconstruction algorithm. This geometry is currently defined by the manufacturer based on design values and is not measured for each scan. It was noted during DXTTR imaging that the large amount of biting force placed on the bitewing holder, coupled with the rigidity of the DXTTR mounting structure, caused some torsion in the holder. This was also noted by presence of the collimator edge in the projection images and inevitably caused some small deviation in the actual source/detector geometry compared to the design values. A more rigid bitewing holder could be implemented for patient use, although the patients will have more degrees of freedom than the fixed mounting bracket of the DXTTR. The actual impact of mechanical deformation on image quality will be assessed during patient trials.

4.D. Collimation

The radiation field of the s-IOT device meets FDA requirements for collimation, with a maximum dimension of 5.2 across the diagonal. The area of the field is only 10 cm^2, corresponding to only 26% of the allowable area of 38 cm^2. Use of the coupled detector holder allows for tight collimation orthogonal to the scan direction and reduction of unnecessary patient exposure.

4.E. Image quality

Various dental models were imaged to demonstrate the conspicuity of dental anatomic features and pathoses. The results shown in this study are examples of potential clinical applications. Reader studies are in progress for several of these lesion types and will better clarify the diagnostic efficacy of s-IOT.

4.E.1. RMI phantom

Reconstruction images of the RMI phantom displayed good visualization of the simulated caries lesions, fractures, buccal, and palatal roots. In 2D periapical imaging, buccal

FIG. 15. (a) 2D image of a dilacerated root specimen; (b,c) Reconstruction slice images of the same specimen in different planes of focus, indicating orientation in a buccal direction.
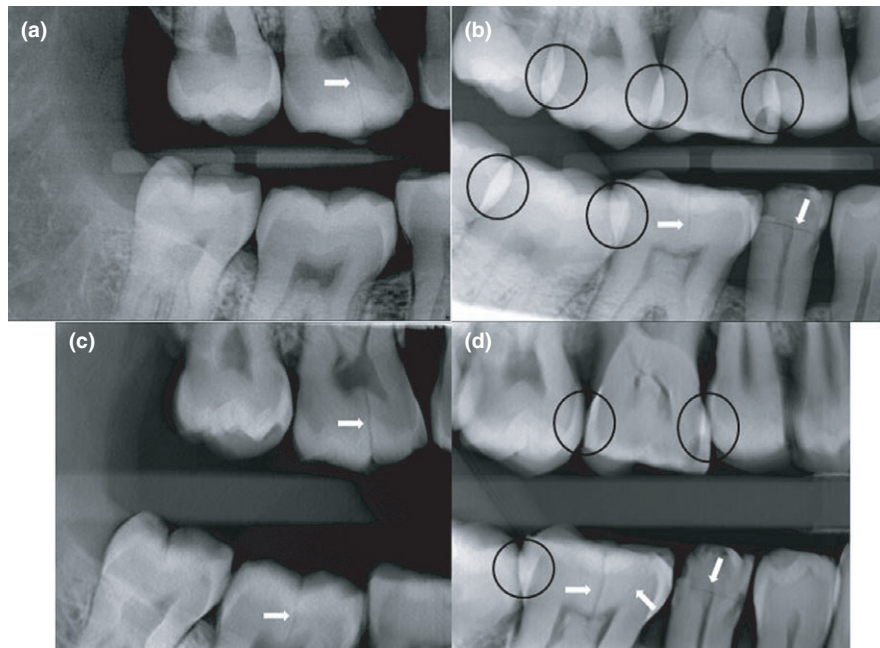
FIG. 16. 2D images (top) and reconstruction slice images (bottom) from DXTTR bitewing acquisition. Reconstruction slices reveal more fractures (arrows), with higher contrast. Interproximal superposition (circled) in the 2D premolar image (b) is eliminated in the corresponding reconstruction slice (d).

and palatal roots overlap which can complicate their independent visualization. The mandibular bone displays good contrast of alveolar porosity in the reconstruction images and implies possible application in evaluation of periodontal bone loss and other disorders presenting as subtle radiolucencies.[1]

4.E.2. Fractured root specimens

Root fracture detection in 2D intraoral radiography is difficult due to the superposition of bone, presence of endodontic obturation materials, and other tooth roots. Root fractures themselves can only be visualized when the fracture plane happens to be parallel to the direction of x-ray propagation.[1] If a fracture is left untreated, the condition will worsen and can lead to severe periodontal problems and tooth loss.

The fractured root specimens were imaged with the x-ray scanning direction at different orientations with respect to the longitudinal axis of the root. Sixty specimens have been imaged on this system for a reader study, currently underway at the UMN School of Dentistry, to assess the sensitivity of the s-IOT for root fracture identification compared to 2D and CBCT imaging modalities. For these two particular specimens shown, the fractures were easily visualized in the reconstruction slice images compared to the corresponding 2D radiographs. The reconstructed images presented in this work were obtained from tomosynthesis scans performed in the standard orientation, with the sample flat on the detector and scanning direction orthogonal to the root axis. Inspection of reconstruction images revealed that varying the sample orientation with respect to the source array provides additional information about the specimen, and multiple-view tomosynthesis may prove to be a valuable resource for diagnostic imaging. Geometrical relationships, including relative depth

and direction of propagation of the fractures, are also easily accessible when viewing the entire reconstruction stack. The fractures are also typically visible in one or more of the basis projection images due to the range of angulation. s-IOT may increase the likelihood of fracture detection by acquiring images from many angles compared to a single 2D intraoral radiograph.

4.E.3. Dilacerated root specimen

Dilacerated roots are a concern in endodontic treatment, orthodontic movement, or surgical extraction. Lack of awareness of the severity and direction of curvature can lead to complications during such procedures. The sample reconstruction images of the dilacerated root specimen clearly show that the root is curved and extends six slices (>3 mm) from the expected location. The contrast in the reconstruction image is excellent, although the specimen was not mounted in bone-simulant and contained only a few millimeters of simulated soft tissue. Not only does s-IOT depict the severity of curvature, but it also provides information about direction of curvature in three-dimensional space that 2D imaging may omit.

4.E.4. Interproximal caries detection

The DXTTR bitewing reconstruction slice images demonstrate good visualization of crown fractures. Scrolling through the reconstruction stack allows the reader to open the contact points between the teeth, effectively removing the acquisition error. Conventional interproximal caries detection relies on proper positioning to ensure open contacts and improper positioning can result in retakes of 2D radiographs.

The use of s-IOT for interproximal caries detection may eliminate the need for retakes by producing pseudo-open contacts. In viewing the reconstruction stack, the tooth cusps are also easily isolated among different reconstruction slices. Early stage, or incipient occlusal caries are difficult to detect with 2D intraoral imaging due to the superposition of tooth cusps. Ex vivo reader studies for interproximal and occlusal caries detection are currently under way at the UNC School of Dentistry.

4.E.5. Image quality and dose

In all image sets, the tomosynthesis reconstruction slices provided more anatomical detail with higher spatial resolution and feature conspicuity than the 2D intraoral comparison images. Information can be gleaned from the reconstruction data that is not available in the 2D images, such as depth or direction of propagation of a fracture.

Bitewing s-IOT imaging of the DXTTR provides the closest approximation to in vivo patient imaging and incorporates additional challenges over loose specimen imaging. The anthropomorphic design allows use of the bitewing detector holder for true clinical positioning and the tissue-mimicking vinyl "skin" provides additional attenuation. Structure of the oral cavity, particularly curvature of the jaws, restricts the positioning of the detector holder, often forcing a larger object-to-detector distance (ODD). The ODD can be up to 3 cm in the premolar region, therefore increasing apparent focal spot size and magnification. The volume of irradiated material is also greater for the DXTTR, including the bitewing feature of the detector holder, generating scattered radiation, which can impact the contrast and spatial resolution. The strong biting force of the DXTTR phantom also produced some deformation of the bitewing detector holder, possibly altering the actual source-detector relationship. Despite these additional factors that could negatively impact the image quality, the DXTTR reconstruction images were very good with crisp visualization of fractures and interproximal surfaces.

The s-IOT clinical prototype system displays good image quality compared to conventional 2D intraoral images. The dilacerated root specimen images display high feature contrast and low noise in a visual comparison to the other s-IOT images, as expected due to the lack of bone and tissue attenuation. An increase in total dose may be warranted to achieve this level of detail in imaging anthropomorphic specimens and patients. This clinical prototype system is currently configured for a maximum total tomosynthesis dose comparable to the UNC SOD technique for one 2D radiograph using a photostimulable phosphor plate (PSP). This limitation is not a constraint of the system hardware, but as an initial configuration for low-dose s-IOT imaging. Expansion of the exposure range is possible and further investigation is needed for complete dose optimization.

The total x-ray exposure time for the tomosynthesis scan varies from 175 to 350 ms, with a total scan time of approximately 5 s. The limiting factor in scan speed is the detector frame rate. Incorporation of a faster detector is underway and should decrease the imaging time to less than 3 s. The image processing and reconstruction step currently requires approximately 20 s. Ongoing enhancement of the reconstruction algorithm will also result in a reduction of computation time.

5. CONCLUSIONS

The stationary intraoral tomosynthesis clinical prototype has been characterized for dose and spatial resolution. Manufacturer specifications for system output, such as tube current, voltage, and pulse width, were validated. Collimation of the radiation field size was deemed adequate. The system is compact and easy to use with a fast scan time and real-time image reconstruction and dose comparable to that of a single 2D intraoral radiograph. Preliminary dental phantom images have been presented and the level of detail visualized in the s-IOT reconstruction slice images suggests that the s-IOT system will increase the diagnostic yield and will be more successful for clinical applications than standard 2D intraoral imaging without an increase in patient dose.

DISCLOSURES

Otto Zhou has equity ownership and serves on the board of directors of XinVivo, Inc., to which the technologies used or evaluated in this project have been or will be licensed. Jianping Lu has equity ownership in XinVivo. Enrique Platin serves on the advisory board of XinVivo. Some of the authors are inventors of a patent on the licensed s-IOT technology. All of these relationships are under management by the University of North Carolina's COI committees. Laurence Gaalaas is Clinical Officer of XinVivo and earns consulting income from XinVivo, a company that may commercially benefit from this research. This relationship has been reviewed and managed by the University of Minnesota in accordance with its conflict of interest policies.

*Present address: 2659 Superior Dr. NW, Rochester, MN 55901-8533, USA.

a)Author to whom correspondence should be addressed. Electronic mail: credmon@email.unc.edu.

REFERENCES

1. Iannucci J, Howerton L. *Dental Radiography: Principles and Techniques*, 4th edn. St. Louis, MO: Elsevier; 2012.

2. Bagramian R, Garcia-Godoy F, Volpe A. The global increase in dental caries. A pending public health crisis. *Am J Dent*. 2009;21:3–8.

3. Bader J, Shugars D, Bonito A. Systematic reviews of selected dental caries diagnostic and management methods. *J Dent Educ*. 2001;65:960–968.

4. Wenzel A. Bitewing and digital bitewing radiography for detection of caries lesions. *J Dent Res*. 2004;83:C72–C75.

5. Tamse A, Fuss Z, Lustig J, Kaplavi J. An evaluation of endodontically treated vertically fractured teeth. *J Endod*. 1999;25:506–508.

6. Rosen E, Tsesis I, Tamse A, Bjorndal L, Taschieri S, Givol N. Medico-legal aspects of vertical root fractures in root filled teeth. *Int Endod J*. 2012;45:7–11.

7. Gaalaas L, Tyndall D, Mol A, Everett E, Bangdiwala A. Ex vivo evaluation of new 2D and 3D dental radiographic technology for detecting caries. *Dentomaxillofac Radiol*. 2016;45:20150281.

8. Webber R, Horton R, Underhill T, Ludlow J, Tyndall D. Comparison of film, direct digital, and tuned-aperture computed tomography images to identify the location of crestal defects around endosseous titanium implants. *Oral Surg Oral Med Oral Path*. 1996;81:480–490.

9. Webber R, Messura J. An in vivo comparison of diagnostic information obtained from tuned-aperture computed tomography and conventional dental radiographic imaging modalities. *Oral Surg Oral Med Oral Path Oral Radiol Endod*. 1999;88:239–247.

10. Nair M, Nair U, Seyedain A, et al. Correlation of tuned aperture computed tomography with conventional computed tomography for evaluation of osseous healing in calvarial defects. *Oral Surg Oral Med Oral Path Oral Radiol Endod*. 2007;103:267–273.

11. Webber R, Horton R, Tyndall D, Ludlow J. Tuned-aperture computed tomography (TACT). Theory and application for three dimensional dento-alveolar imaging. *Dentomaxillofac Radiol*. 1997;26:53–62.

12. Harase Y, Araki K, Okano T. Diagnostic ability of extraoral tuned aperture computed tomography (TACT) for impacted third molars. *Oral Surg Oral Med Oral Path Oral Radiol Endod*. 2005;100:84–91.

13. Nair M, Webber R, Johnson M. Comparative evaluation of tuned aperture computed tomography(R) for the detection of mandibular fractures. *Dentomaxillofac Radiol*. 2000;29:297–301.

14. Nair M, Nair U, Grondahl HG, Webber R. Accuracy of tuned aperture computed tomography in the diagnosis of radicular fractures in non-restored maxillary anterior teeth- an in vitro study. *Dentomaxillofac Radiol*. 2002;31:299–304.

15. Nair M, Nair U. Detection of artificially induced vertical radicular fractures using tuned aperture computed tomography. *Eur J Oral Sci*. 2001;109:375–379.

16. Nair M, Bezik J. Tuned-aperture computed tomography for detection of induced mid-buccal/lingual alveolar bone defects. *J Periodontol*. 2006;77:1833–1838.

17. Nair M, Tyndall D, Ludlow J, May K. Tuned aperture computed tomography and detection of recurrent caries. *Caries Res*. 1998;32:23–30.

18. Harase Y, Araki KT, Okano T. Accuracy of extraoral tuned aperture computed tomography (TACT) for proximal caries detection. *Oral Surg Oral Med Oral Path Oral Radiol Endod*. 2006; 101:791–796.

19. Nair M, Tyndall D. The effect of restorative material and location on the detection of simulated recurrent caries. A comparison of dental film, direct digital radiography and tuned aperture computed tomography. *Dentomaxillofac Radiol*. 2008;27:80–84.

20. Shi X, Han P. Tuned-aperture computed tomography for detection of occlusal caries. *Dentomaxillofac Radiol*. 2001;30:45–49.

21. Tyndall D, Clifton R, Webber R, Ludlow J, Horton R. TACT imaging of primary caries. *Oral Surg Oral Med Oral Path Oral Radiol Endod*. 1997;84:214.

22. Li L, Chen Z, Zhao Z, Wu D. X-ray intra-oral tomosynthesis for quasi-three-dimensional imaging: system, reconstruction algorithm, and experiments. *Opt Eng*. 2013;52:013201.

23. Ziegler C, Franetzki M, Denig T, Muhling J, Hassfeld H. Digital tomosynthesis - experiences with a new imaging device for the dental field. *Clin Oral Invest*. 2003;7:41–45.

24. Cho M, Kim H, Youn H, Kim S. feasibility study of digital tomosynthesis for volumetric dental imaging. *J Instrum*. 2012;7:P03007.

25. Franetzki M, Guenther W, Ploetz J. X-ray diagnostics installation. US Patent 5598454, 29 Jan 1997.

26. Zhang J, Yang G, Cheng Y, et al. Stationary scanning X-ray source based on carbon nanotube field emitters. *Appl Phys Lett*. 2005;86:184104.

27. Qian X, Rajaram R, Calderon-Colon X, et al. Design and characterization of a spatially distributed multibeam field emission x-ray source for stationary digital breast tomosynthesis. *Med Phys*. 2009;36:4389–4399.

28. Shan J, Tucker AW, Lee YZ, et al. Stationary chest tomosynthesis using a CNT x-ray source array: a feasibility study. *Phys Med Biol*. 2014;60:81.

29. Zhou O, Lu J, Shan J, et al. Intraoral tomosynthesis systems, methods, and computer readable media for dental imaging. US Patent 9,782,136, 10 October 2017.

30. Shan J, Tucker A, Gaalaas L, et al. Stationary intraoral digital tomosynthesis using a carbon nanotube x-ray source array. *Dentomaxillofac Radiol*. 2015;44:20150098.

31. Mol A, Gaalaas L, Platin E, et al. Intraoral tomosynthesis using carbon nanotube (CNT) X-ray technology: Primary caries detection. Indianapolis, IN: American Academy of Oral and Maxillofacial Radiology; 2015; Abstract 41: p. 21.

32. NCT02873585. ClinicalTrials.gov. NIH, 16 June 2017. https://clinicaltrials.gov/ct2/show/NCT02873585. Accessed 1 August 2017.

33. Gonzales B, Spronk D, Cheng Y, et al. Rectangular fixed-gantry CT prototype: combining CNT X-ray sources and accelerated compressed sensing-based reconstruction. *IEEE Access*. 2014;2:971–981.

34. 21CFR1020.31, Code of Federal Regulations Title 21, vol. 8, Chapter I, Subchapter J; rev. 01 April 2017. https://www.accessdata.fda.gov/scripts/cdrh/cfdocs/cfcfr/CFRSearch.dfm?FR=1020.31.

35. Samei E, Flynn M, Reimann D. A method for measuring the presampled MTF of digital radiographic systems using an edge test device. *Med Phys*. 1998;25:102–113.

36. Colombo P, Radici L, Torresin A, Pasetto S. Artifact analysis in digital breast tomosynthesis (DBT), European Society of Radiology, C-1006, ECR 2013. https://doi.org/10.1594/ecr2013-c-1006

37. North Carolina Adminstrative Code. 10A NCAC 15 .0604 General requirements for all diagnostic systems; 2015.